Investigation the Influence of the Welding Seams Trajectory on Driving Energy for Industrial Robots

Duong Xuan Bien(✉)

Le Quy Don Technical University, Hanoi, Vietnam
duongxuanbien@lqdtu.edu.vn

Abstract. This paper focuses on investigating the effect of the welding seams in the working space on the driving energy for the six degrees of freedom (6DOF) FD-V8 industrial welding robot. The system of kinematics equations is built on the basis of multi-bodies mechanics theory and industrial robotics theory. The AGV algorithm is applied to solve the inverse kinematics problem (IKP) for each specific welding seam. The Lagrange - Euler method is used to build the differential equations of the robot motion. The robot driving energy is determined on the basis of solving the inverse dynamics problem (IDP). The results of this study have important implications in designing an appropriate welding seams trajectory to reduce energy consumption, as a basis for step by step building the optimizing energy consumption and production costs problem meeting the challenge of the current energy shortage in modern industrial production.

Keywords: Industrial robots · Welding seam · Driving energy

1 Introduction

Smart manufacturing is the core of industrial revolution 4.0. In particular, industrial robots in general and welding robots, in particular, are one of the main subjects that are interested in research and application more and more. The need to improve the performance of robots is always an urgent issue. In the current and near future, the number of robots will be used large, with continuous operation frequency and long working cycles in smart factories. Therefore, they are subject to high energy consumption in production. Finding solutions to reduce energy consumption is an urgent matter in order to minimize costs and enhance production efficiency.

The problem of reducing costs and improving machining productivity of robots is solved in many directions such as optimization of machining trajectory [1–3], feed rate [4–6], technology parameters [7–9] and reduction of machining time leads to reduced energy consumption during machining [10–12].

The optimization direction of production planning, operation based on optimization of production processes, management of delay time, waiting time, and operation time is an important and key direction studied by most enterprises. However, this solution

N. V. Khang et al. (Eds.): ASIAN MMS 2021, MMS 113, pp. 910–920, 2022.
https://doi.org/10.1007/978-3-030-91892-7_87

depends heavily on the specific conditions of the management level, the external organization but has not yet entered into the operational nature of each production equipment. The optimal research direction of the technology parameters depends a lot on the object of processing. The technological parameters change continuously when changing materials, textures of objects, and machining methods [7–9]. In order to find the optimal parameters, it is necessary to carry out many tests, measurements, and statistics, which consumes time and research costs. The research direction to optimize the energy consumption based on the optimal trajectory, jerk, and feed rate goes into the nature of the kinematics and dynamics of the robot, which is feasible and highly cost-effective. These methods are implemented based on basic researches right in robot structure design, trajectory design, and optimization algorithms.

The issue of energy consumption in production is directly mentioned in [13–20]. Experimental studies on the effects of robot operating factors on energy consumption are discussed in [10]. The algorithm that minimizes the energy required to move in a point-to-point trajectory is proposed by [11] and applies the simulation for a 2DOF planar robot. The issue of energy consumption for a system of many robots is examined in [12] with a 3DOF robot used to illustrate the algorithm. The technique for adjusting the parameters of the dynamics model and recognition technology is used in [13] to plan the trajectory of industrial robots with the minimum energy consumption. The problem of evaluating the effects of feed rate and load on energy consumption is mentioned in [14] through the construction of an industrial robot simulation model. Determining the optimal positions in the robot workspace to minimize the driven energy is considered in [15]. Similarly, using energy efficiency is considered for the 4-DOF parallel robot in [16] based on the position optimization in the workspace. The energy consumption optimization solution through the structural optimization design study considered in [17], the 5-bar mechanism model and the SCARA robot are the illustrated objects. The redundant properties of the robot in [18] are exploited to improve the efficiency of driving energy. In essence, this proposal is also based on adjusting the machining trajectory of the robot. The proposed model for calculating the energy consumption of the robot with the effect of temperature at the robot's driving joints is presented in [19]. The solution to reduce energy consumption for the pick-and-drop robot based on the optimal working trajectory is also presented in [20]. Energy consumption in the production process has been studied for a long time, but mainly focused on the cutting process on CNC machines, but mainly through experimental research. For industrial robots, this issue has only been interested in recent years due to the development and application of more and more robots in industrial production, the explosion of the industrial revolution 4.0, and the challenge of the global energy shortage.

This paper focuses on surveying the effect of the welding seams in the workspace on the driving energy of the robot joints. This driving energy is described in terms of the torque value of each joint. The robot mathematical model is built using the multi-bodies mechanics theory and industrial robot theory. The welding seams in the workspace are used as an input for the IKP to determine the values of the joint variables. The AVG method [21] is effectively used to solve the IKP. The dynamics equations are established based on the energy differential equations Lagrange - Euler. The driving torques of joints are determined by solving the IDP.

2 Materials and Methods

2.1 The Kinematics and Dynamics Modeling

Consider the kinematics model of industrial welding robot FD-V8 with 6DOF as shown in Fig. 1. The fixed coordinates system is $(OXYZ)_0$ located at point O_0 and $(OXYZ)_i$, $(i = 1 \div 6)$ are the local coordinate systems attached link i. Table 1 describes the kinematic parameters according to the D-H rule [23]. Accordingly, the transformation homogeneous matrices $\mathbf{H}_i$, $(i = 1 \div 6)$ are determined.

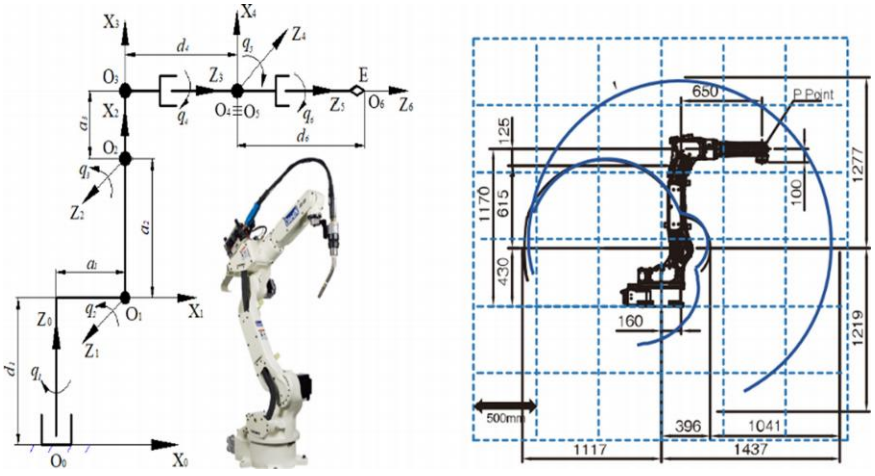

Fig. 1. Kinematic model of the FD-V8 robot and the EEP working range [22]

Table 1. DH parameters

Links	DH parameters			
	$\theta_i = q_i$	d_i	a_i	α_i
1	q_1	d_1	a_1	$\pi/2$
2	q_2	0	a_2	0
3	q_3	0	a_3	$\pi/2$
4	q_4	d_4	0	$\pi/2$
5	q_5	0	0	$-\pi/2$
6	q_6	d_6	0	0

The position and direction of the end-effector point (EEP) from the $\mathbf{D_6}$ matrix following the fixed coordinate system are determined as follows [23]. In this paper, the tip point of the welding torch is the end-effector point.

$$\mathbf{D}_6 = \mathbf{H}_1\mathbf{H}_2\mathbf{H}_3\mathbf{H}_4\mathbf{H}_5\mathbf{H}_6 \tag{1}$$

Define the generalized vector of robot is $\mathbf{q} = [q_1 \ q_2 \ q_3 \ q_4 \ q_5 \ q_6]^T$ and $\mathbf{x}_{EEP}(t) = \begin{bmatrix} x_E & y_E & z_E \end{bmatrix}^T$ is the coordinate vector of end-effector point following fixed

coordinate system. The forward kinematics equations can be written as

$$\mathbf{x}_{EEP} = f(\mathbf{q}) \tag{2}$$

Where, f is a vector function representing the robot forward kinematics. Derivative (2) with respect to time, the relation between generalized velocities is obtained as

$$\dot{\mathbf{x}}_{EEP} = \mathbf{J}(\mathbf{q})\dot{\mathbf{q}} \tag{3}$$

Where, $\mathbf{J}(\mathbf{q})$ is the Jacobian matrix with size 3×6. The acceleration of the end-effector point can be given by derivation (3)

$$\ddot{\mathbf{x}}_{EEP} = \dot{\mathbf{J}}\dot{\mathbf{q}} + \mathbf{J}\ddot{\mathbf{q}} \tag{4}$$

The IKP equations of robots are written as

$$\mathbf{q} = f^{-1}(\mathbf{x}_{EEP}) \tag{5}$$

The values of vector $\mathbf{q}$ have been determined from (5), the joints velocity is determined as

$$\dot{\mathbf{q}} = \mathbf{J}^{+}(\mathbf{q})\dot{\mathbf{x}}_{EEP} \tag{6}$$

Where, $\mathbf{J}^{+}(\mathbf{q})$ is the pseudo-inverse matrix of $\mathbf{J}(\mathbf{q})$ matrix and is defined as [23]

$$\mathbf{J}^{+}(\mathbf{q}) = \mathbf{J}^{T}(\mathbf{q})\left[\mathbf{J}(\mathbf{q})\mathbf{J}^{T}(\mathbf{q})\right]^{-1} \tag{7}$$

The joints acceleration is calculated from (6)

$$\ddot{q} = \mathbf{J}^{+}(\mathbf{q})(\ddot{x}_{EEP} - \dot{J}\dot{q}) \tag{8}$$

For the given $\mathbf{x}$, $\dot{\mathbf{x}}$, $\ddot{x}$ vectors and using the algorithms for adjusting the increments of generalized vector which was proposed in [21], the approximately joint variables value can be determined exactly. The dynamics equations show the relationship between forces and torques with the motion characteristics of robots such as joint position $\mathbf{q}$, velocity $\dot{\boldsymbol{q}}$, joint acceleration $\ddot{q}$. The dynamics equations of the robot are described as follows [24]

$$\mathbf{M}(\mathbf{q})\ddot{q} + \mathbf{C}(\mathbf{q}, \dot{\mathbf{q}})\dot{\boldsymbol{q}} + \mathbf{g}(\mathbf{q}) = \tau \tag{9}$$

Where, $\mathbf{M}(\mathbf{q})$is the mass matrix, $\mathbf{C}(\mathbf{q}, \dot{\mathbf{q}})$ is Coriolis matrix, $\mathbf{g}(\mathbf{q})$is the gravity vector, τ is the joints torque vector. The components of (9) are determined similarly in [24]. The generalized vectors $\mathbf{q}$, $\dot{\mathbf{q}}$, $\ddot{q}$ and $\dddot{q}$ are calculated from solving the IKP.

2.2 The IKP and IDP

Due to the robot is a redundant system solving the system of (5) will give countless answers. Choosing the most suitable answer is a quite difficult problem. Therefore, building an effective algorithm to solve the problem of inverse kinetics is always interested in. Apply the AGV algorithm [21] to find $\mathbf{q}(t)$ value with given rules $\mathbf{X}_{EEP}(t)$, $\dot{X}_{EEP}(t)$, $\ddot{X}_{EEP}(t)$. The position error $\mathbf{e}_{\mathbf{X}}$ of the EEP can be determined as follows

$$\mathbf{e}_{\mathbf{x}} = \mathbf{x}_{EEP} - f(\mathbf{q}) \tag{10}$$

The dynamic problem includes the forward and inverse dynamics. The forward dynamic problem has input data that are driving torques or forces and outputs are the dynamic behaviors such as the position, velocity, and acceleration of the joints in the joint space or the EEP in the workspace. The inverse dynamics allows determining the value of torques or driving forces required to ensure that the motion of the system according to the given path $\mathbf{x}_{EEP}(t)$ in the workspace or $\mathbf{q}(t) = \left[q_1\ q_2 \ldots\ q_6 \right]^T$ in the joint space. Solving the inverse dynamic problem in the workspace is truly complicated because it is necessary to solve before the already complicated IKP.

The driven torque vector can be found as follows

$$\boldsymbol{\tau}(t) = \mathbf{M}(\mathbf{q})\ddot{\mathbf{q}} + \mathbf{C}(\mathbf{q}, \dot{\mathbf{q}})\,\dot{\mathbf{q}} + \mathbf{g}(\mathbf{q}) \tag{11}$$

The calculational diagram for solving the IDP is described as Fig. 2.

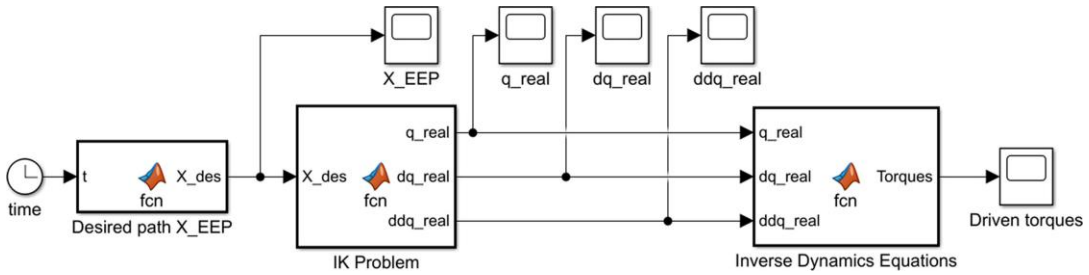

Fig. 2. The calculation diagram for the inverse dynamic problem in MATLAB/SIMULINK

2.3 Numerical Simulation Results and Discussions

This section presents the numerical simulation results for welding robot FD-V8 with three weld seams. Some dynamics parameters of the system can be showed as Table 2.

Table 2. Dynamics parameters of the system

No	Link 1	Link 2	Link 3	Link 4	Link 5	Link 6
Length of links (m)	0.42	0.15	0.56	0.13	0.6	0.325
Mass of links (kg)	127.9	37.4	79.9	19.2	3.8	3.7
Inertial moment of links (I_{xx}) (kg.m^2)	2.26	0.064	0.76	0.81	0.022	0.04
Inertial moment of links (I_{yy}) (kg.m^2)	3.04	1.25	0.88	0.78	0.0045	0.031
Inertial moment of links (I_{zz}) (kg.m^2)	2.49	1.281	0.95	0.075	0.021	0.011

Given the welding seams of the EEP in three cases are shown in Table 3.

Table 3. Trajectories in the workspace

Trajectory	$x_E(m)$	$y_E(m)$	$z_E(m)$
Case 1	$0.7 + 0.3\sin(2t)$	$0.3\cos(2t)$	0.45
Case 2	0.7	$0.3\cos(2t)$	$0.65 + 0.3\sin(2t)$
Case 3	$1.075 + 0.3\sin(2t)$	0	$0.81 + 0.3\cos(2t)$

Three welding seams in these basic planes are used to determine the torques of a redundant manipulator with 6DOF fixed in a vertical plane. There are many different types of trajectories in space depending on the specific task and these are all based on the three basic planes. The position, velocity, and acceleration of the joints are the results of this problem. The IKP solving algorithm takes the given error of the joints variables and limits the joints as the conditions for performing the calculation. There are several reasons for choosing 3 basic planes for planning the EEP trajectory in the workspace. Firstly, this study is only at the beginning of research on the driven torques of robots with simple and basic trajectories. Secondly, parameters of the EEP trajectories on these 3 planes can ensure to bring the EEP of the robot to the positions that need to be investigated such as the position outstretched, close to the robot's body, the position of rising or falling low close to the base. Thirdly, the EEP trajectories are easily built on these basic planes and easily verify reliability in both theoretical and experimental geometry calculations. On the other hand, easily fabricate auxiliary equipment such as jigs for experimenting, measuring, and verifying calculation results. Next, the analysis results of the problem in this paper can be used immediately because in reality most welded structures are mainly machined on these planes. Finally, the generalized EEP trajectory in the workspace can completely be built and investigated, but verifying the reliability and accuracy of the calculations will be a huge challenge, especially experimentally verified.

The numerical simulation results of case 1 with the trajectory in the workspace, the value of joint variables and simulation model in MATLAB are described respectively in Figs. 3, 4, and 5. Similar, simulation results of case 2 are shown in Figs. 6, 7, and 8.

Case 1 (C1): The trajectory on OXY plane.

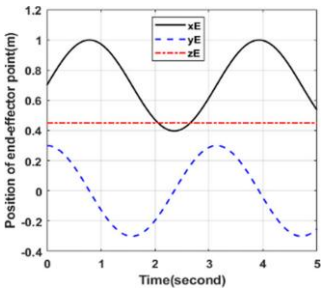

Fig. 3. Trajectory in C1

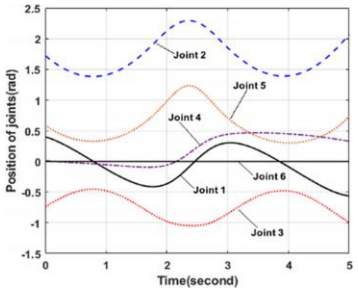

Fig. 4. Joint position in C1

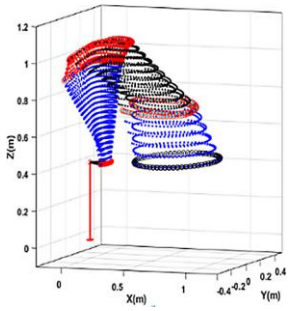

Fig. 5. Case 1

Case 2 (C2): The trajectory on OYZ plane.

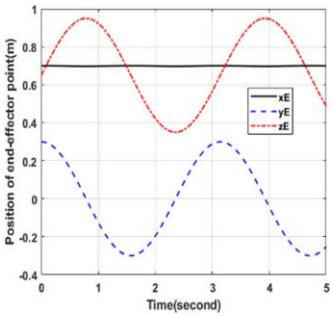

Fig. 6. Trajectory in C2

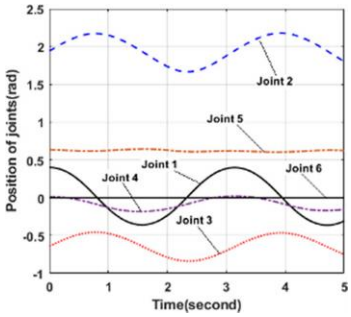

Fig. 7. Joint position in C2

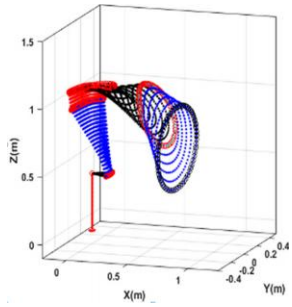

Fig. 8. Case 2

Case 3 (C3): The trajectory on OXZ plane.

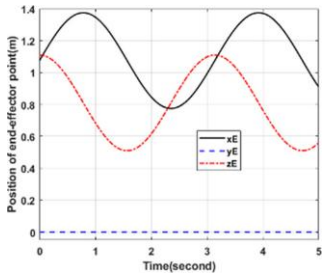

Fig. 9. Trajectory in C3

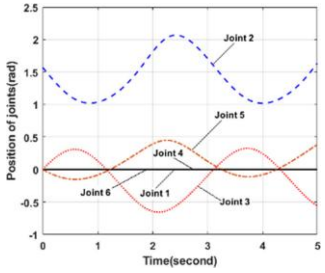

Fig. 10. Joint position in C3

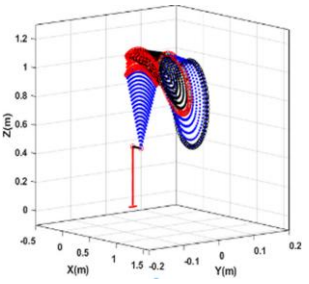

Fig. 11. Case 3

Case 3 is determined in Figs. 9, 10, and 11, respectively. It is easy to see that the values of the joint variables change continuously and there is no singularity point. The 3D model in MATLAB of the robot in Figs. 5, 8 and 11 is created from joint variable values obtained in the IKP solving.

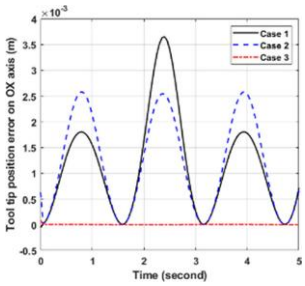

Fig. 12. Error position OX

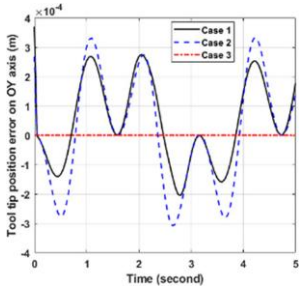

Fig. 13. Error position OY

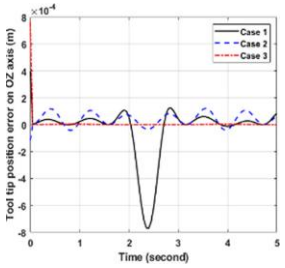

Fig. 14. Error position OZ

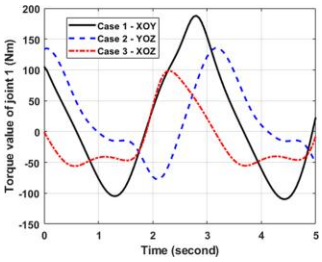

Fig. 15. Torque of q_1

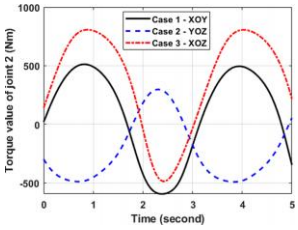

Fig. 16. Torque of q_2

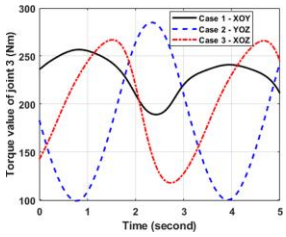

Fig. 17. Torque of q_3

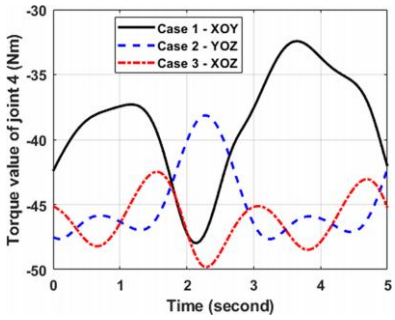

Fig. 18. Torque of q_4

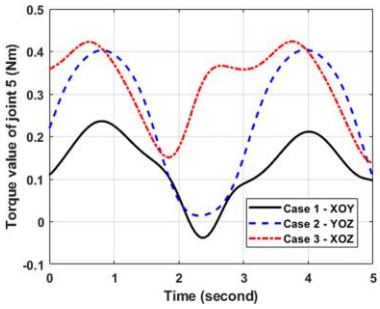

Fig. 19. Torque of q_5

The errors position of the EEP in the workspace are presented in Figs. 12, 13 and 14. The values of errors position are small. Those results prove the high reliability and efficiency of the AGV algorithm. The results of the IDP are the driving torques of joints values that are described from Figs. 15, 16, 17, 18 and 19. For C1-XOY, the maximum driving torque value is 500 (Nm) and is located at joint 2. Likewise, the torque at joint 2 in C2-YOZ and C3-XOZ also reaches the maximum values are 806.8 (Nm) and 297.6 (Nm).

The maximum driving torque value in all cases belongs to joint 2 in C3-XOZ with 806.8 (Nm). This means that the drive motor of joint 2 needs the most drive power. The reason C3 reaches the maximum value is because the robot links must reach the farthest

Table 4. The maximum torque values of joints (Nm)

No	Joint 1	Joint 2	Joint 3	Joint 4	Joint 5	Maximum
Case 1 - XOY	188	500	256.8	48	0.24	500
Case 2 - YOZ	135.5	297.6	285.1	47.7	0.4	297.6
Case 3 - XOZ	97.6	806.8	267	50	0.42	806.8
Maximum	188	806.8	285.1	50	0.42	

from the fixed origin position. The C2-YOZ gives a much smaller torque value than the other two cases. Table 4 presents the maximum torque value of each joint in three cases.

For each specific joint, the maximum driving torque value in joint 1 reaches 188 (Nm) and belongs to C1–XOY. Joint 2 requires the maximum drive torque as described above. Joint 3 gives the same driving torque value in all 3 cases. Joint 4 and joint 5 require a much smaller value of driving torque than joint 1. Joint 5 has the smallest torque value because it only carries the link 6.

In summary, the order of the links with the torque value from the largest to the smallest is joint 2, joint 3, joint 1, joint 4 and finally joint 5, respectively. The torque at the joints is greater when joint the further the operation moves away from the fixed origin. The C2-YOZ gives the driving torque value at the joints is the similarity, does not make a big difference between the joints. Thus, in order to design the welding trajectory to ensure that the driving energy is not too large, the trajectories should be designed according to the C2-YOZ. All cases where there is a change of the OX axis coordinates lead to a high demand for driving power.

3 Conclusion

In general, the effect of the welding path trajectories on the basic planes in the workspace on the driving energy of 6DOF industrial robot has been specific considered and evaluated. The results show that welding trajectories that change in the direction far away from the fixed coordinate system origin require large driving moments. On the other hand, the welding trajectory designed on the YOZ plane (Case 2) requires the smallest driving torque compared to the other cases. The value of the driving torque at joint 2 is always the largest requirement in all cases. This is the basis for calculating and selecting the driving motor power when designing the transmission, calculating the structural strength and cost expected when investing in manufacturing.

References

1. Liu, Y., Tian, X.: Robot path planning with two-axis positioner for non-ideal sphere-pipe joint welding based on laser scanning. Int. J. Adv. Manuf. Technol. **105**(1–4), 1295–1310 (2019). https://doi.org/10.1007/s00170-019-04344-3
2. Liu, F., Lin, L.: Time-jerk optimal planning of industrial robot trajectories. Int. J. Robot. Autom. **31**, 1–7 (2016)

3. Dai, C., Lefebvre, S., Yu, K.M., Geraedts, J.M.P., Wang, C.C.L.: Planning jerk-optimized trajectory with discrete time constraints for redundant robots. IEEE Trans. Autom. Sci. Eng. **17**, 1711–1724 (2020)
4. Liang, F., Zhao, J., Ji, S.: An iterative feed rate scheduling method with confined high-order constraints in parametric interpolation. Int. J. Adv. Manuf. Technol. **92**(5–8), 2001–2015 (2017). https://doi.org/10.1007/s00170-017-0249-6
5. Mansour, S.Z., Seethaler, R.: Feedrate optimization for computer numerically controlled machine tools using modeled and measured process constraints. J. Manuf. Sci. Eng. Trans. ASME **139**, 1–9 (2017)
6. My, C.A., Bien, D.X., Tung, B.H., Cong, N.V., Hieu, L.C.: New Feed Rate Optimization Formulation in a Parametric Domain for 5-Axis Milling Robots. Springer International Publishing, New York, 1121 (2020)
7. Sterling, T., Chen, H.: Robotic welding parameter optimization based on weld quality evaluation. In: 6th Annual IEEE International Conference Cyber Technology Automatic Control Intelligent System IEEE-CYBER 2016, pp. 216–221 (2016)
8. Yan, S.J., Ong, S.K., Nee, A.Y.C.: Optimal pass planning for robotic welding of large-dimension joints with deep grooves. Proc. CIRP **56**, 188–192 (2016)
9. Kumaran, K.S., Raj, S.O.N.: Optimization of parameters involved in robotic MIG welding process based on quality responses. IOP. Conf. Ser. Mater. Sci. Eng **402**, 021016 (2018)
10. Garcia, R.R., Bittencourt, A.C., Villani, E.: Relevant factors for the energy consumption of industrial robots. J. Braz. Soc. Mech. Sci. Eng. **40**(9), 1–15 (2018). https://doi.org/10.1007/s40430-018-1376-1
11. Shugen, M.A.: Real-time algorithm for quasi-minimum energy control of robotic manipulators. In: The 21st International Conference on Industrial Electronics, Control, and Instrumentation (IECON 1995), Orlando, pp. 1324–1329 (1995)
12. Wigstrom, O., Lennartson, B.: Towards integrated OR/CP energy optimization for robot cells. In: IEEE International Conference on Robotics and Automation, Hong-Kong (2014)
13. Paes, K., Dewulf, W., Elst, K.V., Kellens, K., Slaets, P.: Energy efficient trajectories for an industrial ABB robot. Proc. CIRP **15**, 105–110 (2014)
14. Paryanto, Brossog, M., Bornschlegl, M., Franke, J.: Reducing the energy consumption of industrial robots in manufacturing systems. Int. J. Adv. Manuf. Technol. **78**, 1315–1328 (2015)
15. Wolniakowski, A., Valsamos, C., Miatliuk, K., Moulianitis, V., Aspragathos, N.: Optimization of dynamic task location within a manipulator's workspace for the utilization of the minimum required joint torques. Electronics **10**, 1–18 (2021)
16. Scalera, L., Boscariol, P., Carabin, G., Vidoni, R., Gasparetto, A.: Enhancing energy efficiency of a 4-DOF parallel robot through task-related analysis. Machines **1**, 1–14 (2020). https://doi.org/10.3390/machines8010010
17. Palomba, E., Wehrle, G.C., Vidoni, R.: Minimization of the energy consumption in industrial robots through regenerative drives and optimally designed compliant elements. Appl. Sci. **10**(21), 1–18 (2020). https://doi.org/10.3390/app10217475
18. Boscariol, P., Caracciolo, R., Richiedei, D., Trevisani, A.: Energy optimization of functionally redundant robots through motion design. Appl. Sci. **10**(9), 3022 (2020). https://doi.org/10.3390/app10093022
19. Eggers, K., Knochelmann, E., Tappe, S., Ortmaier, T.: Modeling and experimental validation of the influence of robot temperature on its energy consumption. In: Proceedings of IEEE International Conference Industrial Technology, pp. 239–243 (2018)
20. Pellicciari, M., Berselli, G., Leali, F., Vergnano, A.: A method for reducing the energy consumption of pick-and-place industrial robots. Mechatronics **23**, 326–334 (2013)

21. Khang, N.V., Dien, N.P., Vinh, N.V., Nam, T.H.: Inverse kinematic and dynamic analysis of redundant measuring manipulator BKHN-MCX-04. Vietnam J. Mech. VAST **32**, 15–26 (2010)
22. FD-V8 robot. https://www.daihen-usa.com/product/fd-v8-robot-6kg-payload-1-4m-reach/. Accessed 21 June 2021
23. Spong, M.W., Hutchinson, S., Vidyasagar, M.: Robot Modeling and Control, 1st edn. Wiley, New York (2001)
24. Khang, N.V: Dynamics of Multi-bodies. Hanoi Science and Technology Publishing House (2007)